

# MIXED FLIGHT CONTROL LAYOUT FOR ULTRALIGHT GENERAL AVIATION AIRCRAFT

Marc May<sup>1</sup>, Daniel Milz<sup>1</sup>, Werner Scholz<sup>2</sup>, Peter Herrmann<sup>2</sup>, Jonas Karger<sup>2</sup>, Lars Peters<sup>3</sup>, Niels Mumm<sup>3</sup> & Richard Kuchar<sup>1</sup>

<sup>1</sup>German Aerospace Center (DLR), Münchner Str. 20, D-82234 Weßling, Germany <sup>2</sup>SFL GmbH, Baumwiesenweg 6b, 70569 Stuttgart, Germany <sup>3</sup>Amazilia Aerospace GmbH, Nymphenburger Str. 84, 80636 München, Germany

#### **Abstract**

Ultralight aircraft in the  $120\,\mathrm{kg}$  class (UL-LL in Germany) are characterized by simplicity through strict weight limitation and low administrative effort. Two key factors are appealing but likewise impose safety concerns: UL-LL aircraft neither require an airworthiness certificate nor undergo annual inspections, and pilots are not obliged to pass pilot medical examinations. With the aim to address the accompanying safety issues, a holistic approach is pursued within the *MOREALIS* project, including pilot and aircraft health monitoring, decision making and automatic emergency landing. On the aircraft side, a backup electric flight control system augments mechanical pilot flight controls in case of aircraft degradation or pilot incapacitation. This means that both decoupled flight control systems access separate control surfaces, and control authority has to be shared between the two systems. This paper presents the design of the mixed flight control layout and analyses the remaining flight and handling qualities for each control system with regard to critical flight maneuvers and failure cases. The results show that especially the pitch authority is critical, and pilot handling qualities for both longitudinal and lateral motion are not satisfactory. These issues can be addressed either with a redesign of control surfaces, or a pilot augmentation approach, where the automated surfaces copy pilot surface commands. Despite the decreased performance, the electric flight controls allow to safely land the aircraft in case of pilot medical emergencies, thereby fulfilling the main requirement.

Keywords: Flight Control, Control Authority, General Aviation, Ultralight, Fault-Tolerant Control

#### 1. Introduction

The 120-kg class of ultralight aircraft (UL-LL in Germany) enables entry into aviation with low hurdles for both pilots and manufacturers. Compared to others, UL pilots usually have less training and fewer medical fitness requirements. The certification of a new UL aircraft is also easier for manufacturers, as fewer bureaucratic hurdles and less complex certification procedures are required, i.e., in comparison to CS-23. As a result, UL aircraft are becoming increasingly popular in the aviation sports sector. However, this trend comes at the expense of the high safety requirements typical for aviation [14]. This simplification is compensated for by the obligation to have an emergency parachute. However, this rescue system also has certain disadvantages. On the one hand, the aircraft is in an uncontrolled descent when the parachute is deployed, and can possibly drift into danger zones (e.g. high-voltage power lines) under unfavorable wind conditions. On the other hand, this system can also fail in the event of a medical emergency or cognitive overload of the pilot. Consequently, there remains a residual risk.

The MOREALIS research project aims to address this very problem within a holistic approach, including pilot and aircraft health monitoring, decision making and automatic emergency landing. In case of aircraft degradation, a fault-tolerant controller is intended to assist the pilot and improve ride and handling qualities. In case of pilot incapacitation, however, the same flight controller takes over the entire flight task and allows to perform an automatic emergency landing.

A challenge arises with respect to the realization of actuation. Due to weight, complexity, and cost constraints, aircraft in the UL class usually deploy mechanical flight controls, where pilot controls are directly connected to the control surfaces in the form of cables or rods. In addition to aircraft design considerations, the pilot obtains valuable information from the force feedback of mechanical controls. Conventional autopilot (AP) systems augment the mechanical flight controls by connecting a servo motor to the cable system with a clutch [20]. That means they directly access the primary control surfaces. The autopilot is usually limited in authority, allowing the pilot to overrule the system or to disengage it using the clutch. In contrast, [16, 2] present a stability augmentation system (SAS) that is based on splitted control surfaces to obtain two separate automatic and manual flight control systems. While primary intentions of the respective augmentation system may be, i.e., the reduction of pilot workload, the reduction of structural loads, or the improvement of ride qualities [18], the overall aim is always to improve flight safety. In contrast to the augmentation systems, fly-by-wire (FBW) control systems digitally process pilot control inputs and sensor measurements to derive primary (and secondary) control surface deflection commands, which are realized by the respective electromechanical or hydraulic actuators. That allows to include flight envelope protections and fault-tolerant control approaches in the software [19, 8]. In order to achieve similar reliability like mechanical flight controls, hardware redundancy has to be exploited. While more than triplex redundancy is industry standard for airliner flight control computers (FCC), commercial FBW aircraft are also often overactuated, meaning they posses redundant primary control surfaces and additional secondary control surfaces for augmentation. In addition, the actuation system is usually redundant and two actuators are attached to the same control surface.

Although UL-LL aircraft do not require an airworthiness certificate, design flexibility of the control system is especially limited due to the  $120\,\mathrm{kg}$  empty weight constraint (compare [10]) and production costs. The additional components required for the autopilot system, especially the clutch, lead to an excessive increase in empty weight. The same accounts for the FBW system because of the redundancy requirement, which also increases the costs significantly. Implementing an additional automated flight control system next to the mechanical flight controls (similar to [16]) circumvents the redundancy requirements of the "full" FBW solution, and thereby the weight penalties. In case of malfunction, the pilot can simply disengage the power supply of the automated system and remain with manual controls.

With the intention to assess the performance of the mixed flight control layout, the remaining control authority of both separate systems shall be investigated. During aircraft design, especially when sizing the control surfaces, the goal is to provide sufficient control authority in order to comply with handling quality requirements for maneuvers, like US Mil Specs (MIL-F-8785C) [11] and US Mil Stan. (MIL-STD-1797) [12], or to fulfill airworthiness requirements like FAR (Federal Aviation Requirements) [6] or JAR (European Joint Aviation Requirements) [5]. Although providing inside into handling qualities, the Cooper-Harper rating scale [4] is subjective and not applicable for the automated control system. Based on design and certification requirements, Chudoba and Cook [3] identify a set of design-constraining flight conditions that determine control surface sizing. A similar approach is presented in [9], but here analytic estimations are derived for the respective maneuvers to assess stability and control. Goman et al. [7] derives stability maps within trim analysis to investigate the maneuver parameter space of fighter aircraft. In [17], the design of control surfaces for a fixed-wing UAV is derived from maneuver requirements.

This paper presents the design of the mixed flight controls concept for safety augmentation, and assesses the remaining control authority for both respective flight control systems by investigating flight and handling characteristics during critical flight maneuvers. Further, the impact of failure (including hardover) in either automated or manual system are analyzed. In contrast to rudder and elevator, the aileron authority allows to vary the control surface ratio as a design variable. A redesign fulfilling minimal roll authority requirements is conducted. Finally, the results and their impact on design and operation of the intended mixed control setup are discussed.

# 2. Flight Control System Layout

The concept of mixed electric and mechanical flight controls for the ultralight aircraft *MORFOIS* is illustrated in Fig. 1. [2] states that "proper surface sizing is essential to a successful separate surface system". The free design variable is the surface size ratio between mechanical and automated system, and has a decisive impact on the flight characteristics of the aircraft. In contrast to [2, 16], both the manual and the augmented flight control system shall be able to take over the full flight task. This suggests a 50:50 distribution of control authority in the initial design. In case of the elevator, this is a hard requirement, as it otherwise limits the flight envelope due to pitch balancing. In contrast, the rudder and aileron do not face these hard demands, and a 50:50 distribution of surface area is initially chosen for simplicity. However, as control authority is distributed more or less equally, hardover failures (according to Roskam and Henry [15], failures where the surface is driven into saturation) in one control system might lead to fading controllability for the other system.

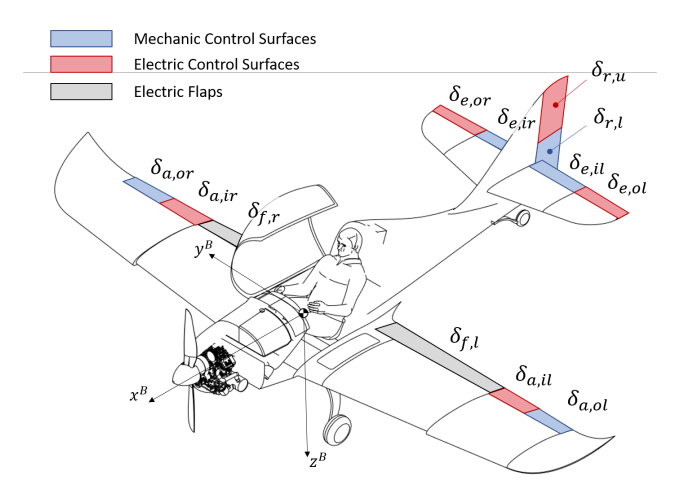


Figure 1 – Concept of mixed flight control layout for ultralight aircraft MORFOIS.

In general, designing an aircraft with the initial intention to include both separate surface flight control systems is beneficial, because the requirements for assembly space and weight constraints are directly included in the design decisions. For the automated flight control system, elevator and rudder are connected to the actuators via lever mechanism, which allows to reduce the load torque and thereby permits to deploy smaller, lighter and cheaper actuators. These are integrated into empennage.

The modular design is likewise applied for the flight control computer, where computation is distributed to a robust, safety-critical FCC intended for the primary flight control task, and an additional companion computer for complex, computation-intensive algorithms developed within the scope of the project.

The control surface deflection limits for elevator  $\delta_e$ , aileron  $\delta_a$ , rudder  $\delta_r$ , and flaps  $\delta_f$  are given in Table 1.

Table 1 – Maximum, minimum, or discrete control surface deflections

$$\begin{array}{c|cccc} \delta_e & \delta_a & \delta_r & \delta_f \\ \hline \pm 20^\circ & \pm 20^\circ & \pm 30^\circ & 0^\circ, 20^\circ, 40^\circ \end{array}$$

### 3. Control Authority Assessment

This chapter presents the evaluation of the flight controls layout. Initially, the flight dynamic model deployed for testing is briefly presented.

#### 3.1 Simulation Setup

The equations of motion (EoM) for 6DoF flight relative to a non-rotating flat earth inertial frame  $\mathscr{F}_E$  are

$$\dot{\vec{v}}^B = \frac{\sum \vec{f}^B}{m} - \vec{\omega}^B \times \vec{v}^B \tag{1}$$

$$\dot{\vec{\omega}}^B = I^{-1} \left( \sum \vec{m}^B - \vec{\omega}^B \times I \vec{\omega}^B \right) \tag{2}$$

with translational  $(\vec{v}^B)$  and rotational  $(\vec{\omega}^B)$  velocities, and force  $(\vec{f}^B)$  and moment  $(\vec{m}^B)$  vectors, all defined in the body frame  $\mathscr{F}_B$ . I and m represent inertia and mass, which depend on the load setting. The contributions of gravitation (G) and propulsion (P) are

$$\vec{f}_G^B = m \cdot \mathbf{R}_{be} \begin{bmatrix} 0 & 0 & g \end{bmatrix}^T \tag{3}$$

$$\vec{f}_P^B = \begin{bmatrix} T & 0 & 0 \end{bmatrix}^T \tag{4}$$

$$\vec{m}_P^B = \begin{bmatrix} \pm Q & 0 & 0 \end{bmatrix}^T + \vec{r}_P \times \vec{f}_P^B \tag{5}$$

 $\mathbf{R}_{be}$  is the rotation matrix from earth to body frame. The propeller axis of rotation is aligned with the body x-axis, and the propeller position relative to the center of gravity (CG) is  $\vec{r}_P$ . The sign of the propeller torque is positive for a negative direction of rotation (with respect to the body x-axis), and vice-versa. As the focus is on the evaluation of the flight controls layout, the basic propeller model is applied for the computation of thrust T and torque Q

$$T = c_T \rho n^2 D^4 \tag{6}$$

$$Q = c_O \rho n^2 D^5 \tag{7}$$

where n denotes revolutions per second,  $\rho$  is air density, and D is the propeller diameter. The prop coefficients  $c_T$  and  $c_O$  vary with the advance ratio  $J = v_x^B/n/D$ .

Effects of propeller slipstream (axial induced velocity, *corkscrew effect*) on the aerodynamics are not considered. The idea is to derive a coefficient model based on panel and strip theory, which can later easily tested within robustness investigation. The ambition of the model is to capture asymmetric control surface deflections, as they might occur during failure scenarios. The coefficients are derivatives of aerodynamic forces and moments with respect to the 19-dimensional aerodynamic state, denoted  $\vec{x}_A$ , which is defined as shown in Table 2:

Table 2 – Components of aerodynamic state  $\vec{x}_A$ 

ID	Variable
1	constant term
2 - 4	$V, \alpha, \beta$
5-7	$p^*,q^*,r^*$
8 - 10	$\delta_{a,ir},\delta_{a,or},\delta_{f,r}$
11 - 13	$\delta_{a,il},\delta_{a,ol},\delta_{f,l}$
14 - 15	$\delta_{e,ir},\delta_{e,or}$
16 - 17	$\delta_{e,il},\delta_{e,ol}$
18 - 19	$\delta_{r,l},\delta_{r,u}$

where V,  $\alpha$ ,  $\beta$  are the absolute velocity, the angle of attack, and the sideslip angle, respectively. For all forces and moments, the aerodynamic state is adapted to include relevant non-linearities. Details are provided in the Appendix.

The resulting aerodynamic forces (D,Y,L) in the aerodynamic frame and moments  $(M_x,M_y,M_z)$ , relative to aerodynamic center AC) in body frame are computed as

$$\vec{f}_A^A = \begin{bmatrix} D & Y & L \end{bmatrix}^T = \frac{\rho}{2} V^2 S \begin{bmatrix} c_D & c_Y & c_L \end{bmatrix}^T$$
 (8)

$$\left(\vec{m}_A^B\right)^{AC} = \begin{bmatrix} M_x & M_y & M_z \end{bmatrix}^T = \frac{\rho}{2} V^2 S \begin{bmatrix} \frac{b}{2} c_{M_x} & \overline{c} c_{M_y} & \frac{b}{2} c_{M_z} \end{bmatrix}^T$$
(9)

Converted to the body frame and applied to the CG, that results in

$$\vec{f}_A^B = \mathbf{R}_{ba} \vec{f}_A^A \tag{10}$$

$$\vec{f}_A^B = \mathbf{R}_{ba} \vec{f}_A^A \tag{10}$$

$$\vec{m}_A^B = \left(\vec{m}_A^B\right)^{AC} + \vec{r}_{\mathsf{AC}} \times \vec{f}_A^B \tag{11}$$

The comparison of strip theory and coefficient model, which can be found in the Appendix, shows an adequate match at three different flight speeds and asymmetric surface deflections.

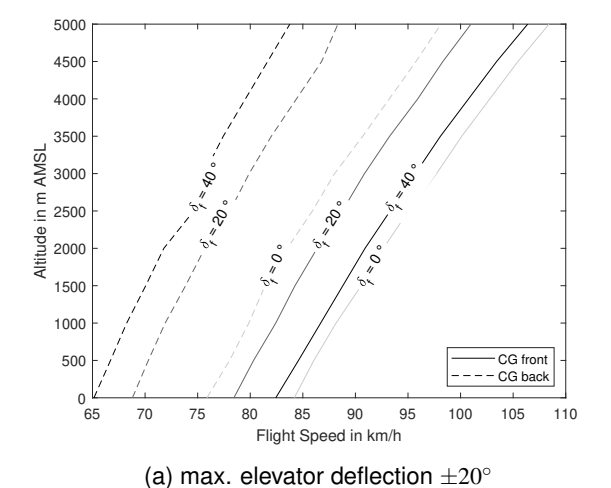
# 3.2 Elevator Authority Assessment

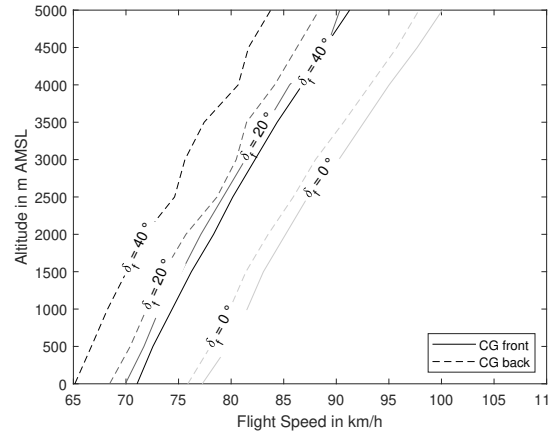
The elevator control authority must ensure stability and controllability throughout the flight envelope. From literature [9], the following three reference flight maneuvers are identified, which allow to determine the suitability of longitudinal control authority.

- · 1-g trimmed flight
- · pitch up/down from trimmed flight
- takeoff control

They are examined in the following.

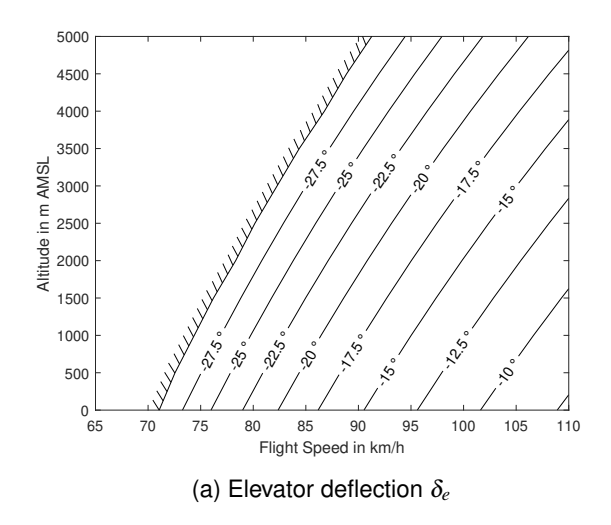
**1-g Trimmed Flight** MIL-F-8785C states that level unaccelerated flight between stall speed  $V_S$  and maximum speed  $V_{\text{max}}$  at all service altitudes shall not be limited by elevator effectiveness. The maximum flight speeds, defined in the initial design, are 200 km h<sup>-1</sup> in nominal conditions and 120 km h<sup>-1</sup> with fully extended flaps. For both, elevator effectiveness is not limited in any way. Therefore, focus is on the lower boundary of the flight envelope. With control surface saturation limits from Table 1, the position of the CG shows to have a strong impact on the size of the flight envelope. The boundaries for front  $(x_{CG} = 1.56 \,\mathrm{m})$  and rear  $(x_{CG} = 1.655 \,\mathrm{m})$  CG positions are plotted in Fig. 2(a). The latter is limited by the maximum angle of attack ( $\alpha_S = 15^{\circ}$ ), wherefore the boundaries coincide with the stall limits. In contrast, for the CG front case, the boundaries are determined by elevator saturation. Due to the impact of flap deflection on the pitch balance, full flap deflections of  $40^{\circ}$  unexpectedly have higher velocity limits compared to flap deflections of 20°. If the operational range of the elevator is extended to  $\pm 30^{\circ}$ , the boundaries for the front CG position are pushed to lower flight speeds. However, for full flap deflection, elevator control authority still is the limiting factor instead of the AoA, see Fig. 2(b). This is demonstrated in Fig. 3, where elevator deflections and the AoA are plotted within the resulting flight envelope for this critical configuration. It can be seen that the boundary coincides with 30° elevator saturation, while the AoA is approximately at 11°, and thus still has some margin to the stall boundary.





(b) max. elevator deflection  $\pm 30^{\circ}$ 

Figure 2 – Flight envelope for front and rear CG position



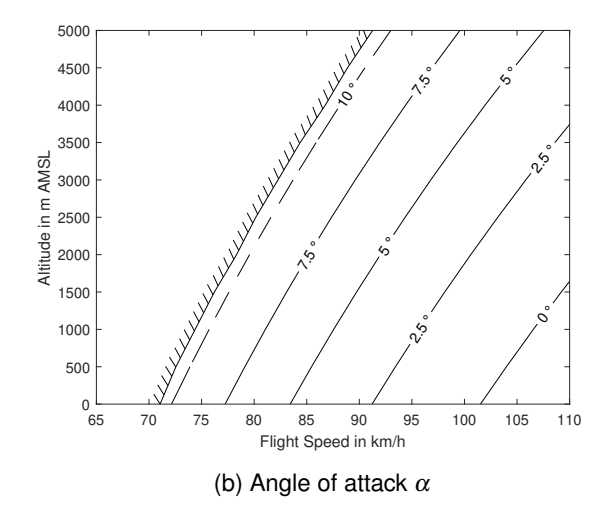


Figure 3 – Trim values for front CG position and  $\delta_f = 40^\circ$ , assuming max. elevator deflection  $\pm 30^\circ$ 

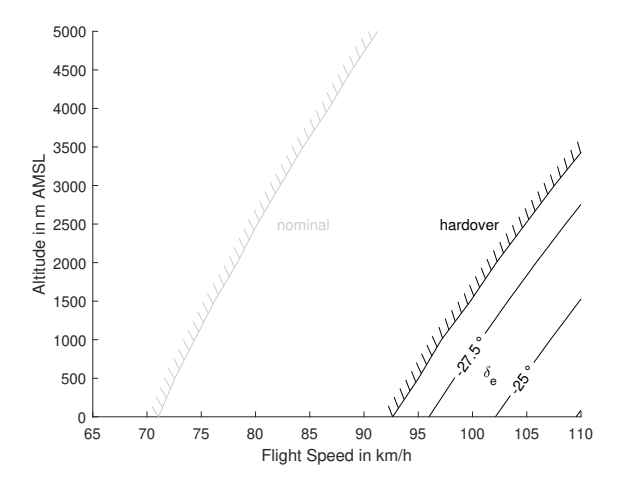


Figure 4 – Reduced flight envelope for front CG position and  $\delta_f = 40^\circ$  for hardover failure in FCS elevator

The basic idea of separated control surfaces was to increase safety. However, electrical actuation is not as reliable as mechanic controls. Therefore, we investigate the impact of a counter-deflected FCS elevator. This faulty behavior might be caused either by erroneous commands from the flight control computer (FCC), or failure in the electric actuators. As the pilot can disengage the FCS/FCC, and thereby suppress failures of this system, we focus our analysis on actuator malfunction. The two FCS elevator surfaces are controlled by separate actuators, wherefore stuck or runaway failures probably occur only on one side. Figure 4 shows the impact of a hardover failure of a single FCS elevator. The flight envelope is drastically reduced, which would result in challenging low speed maneuvers, i.e. during approach. However, the remaining operational FCS elevator surface can be used to neutralize the effect of failure. This introduces a small additional roll moment, which has to be cancelled by appropriate aileron deflections.

In addition to FCS failure, the mechanical pilot elevator inputs might be erroneous, or more specifically countering the FCS commands. This might occur unintentionally when the pilot is in a critical medical condition, e.g. unconscious. As both mechanical elevators are deployed jointly, the resulting countering deflections would have a greater impact compared to the single surface FCS failure, where the latter already showed to be severe in Fig. 4. In case of pilot hardover failures, pitch balancing would not be possible throughout most of the flight envelope, especially concerning the low speed region.

**Longitudinal Maneuvering Flight** MIL-STD-1797 requires that, within the flight envelope, the aircraft should be able to achieve certain pitch load factors from 1-g level flight. The results in Fig. 5, representing again the forward CG case and extended elevator deflection limits, confirm the limited pitch up authority close to the envelope boundary for fully deflected flaps. In contrast, pitching down is favored and shows sufficient load factors.

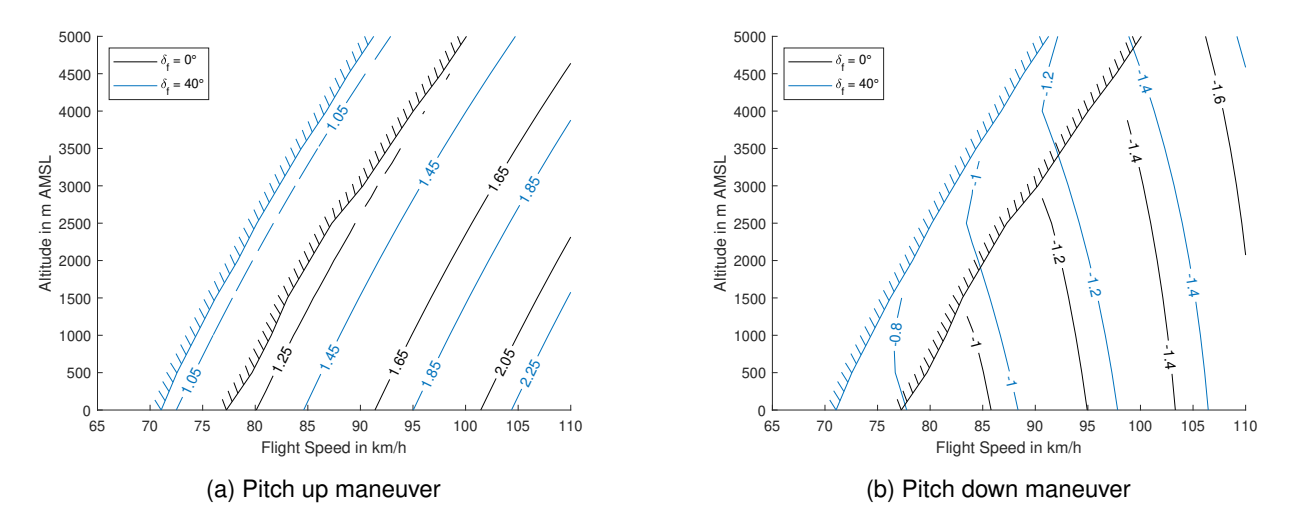


Figure 5 – Minimum/Maximum achievable load factor for pitch down/up maneuvers from trimmed flight, for front CG position, for flaps retracted and fully extended, max. elevator deflection  $\pm 30^{\circ}$ 

**Takeoff Control** For the considered tail-wheel airplane, MIL-F-8785C prescribes that all pitch attitudes until level thrust-line shall be attainable at  $0.5V_S$ . This defines in the lowest takeoff pitch angle of  $0^{\circ}$ , where the fuselage is aligned with the runway. The highest pitch angle during take-off corresponds to the case where the tail wheel still touches the ground, which is  $9^{\circ}$  for the considered configuration (it is assumed that there is no load on the tail wheel). Technically, the automated control surfaces are intended only for emergency landings, wherefore the takeoff maneuver is a mere pilot task to be performed with mechanical controls alone. As shown in Figure 6, the required deflections - when only deploying mechanical surfaces - exceed the design limits. Even for combined deflections, the elevator is close to saturation, but still within limits.

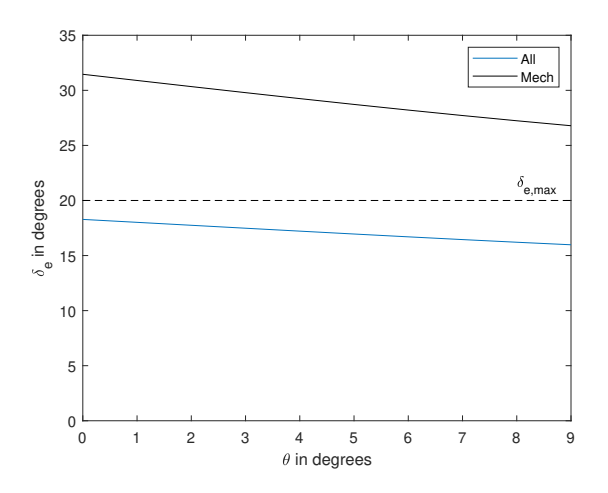
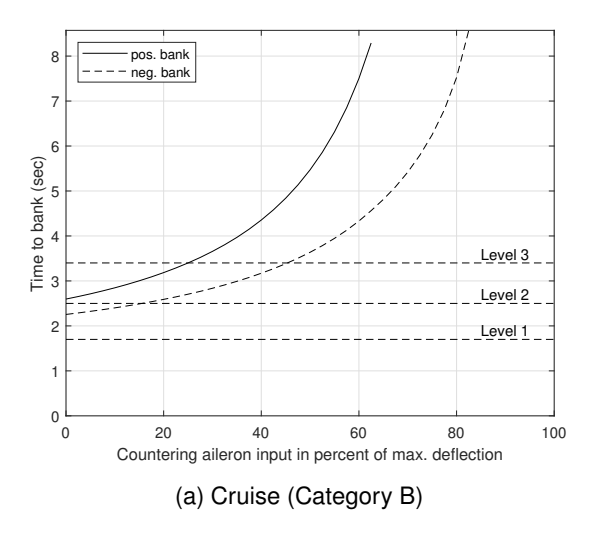


Figure 6 – Trim elevator deflections to hold constant pitch angle  $\theta$  in takeoff conditions at  $0.5V_S$ 

#### 3.3 Aileron Authority Asssessment

The aileron effectiveness is usually assessed by the time to bank, which is either defined to be from wings level to a certain bank angle, or bank to opposite bank angle. While MIL-STD-1797 and MIL-

F-8785C place high demands for adequate handling qualities on the roll time, these are relaxed in CS-VLA 157 to 4 seconds for  $60^\circ$  bank to bank during approach. The requirements have to be fulfilled for both roll directions, respectively. For the considered single-engine aircraft, the propeller torque (assuming a mathematical positive direction of rotation) favors the negative roll dynamics. Consequently, the positive roll motion is the critical case. For both cruise and approach conditions (see Table 3), the roll times achieved by the FCS-assigned ailerons alone ( $2.6\,\mathrm{s}/2.4\,\mathrm{s}$ , see Fig. 7), are between the Level 2 and Level 3 limits defined in MIL-STD-1797, pointing out demanding handling qualities. However, the certification requirements from CS-VLA 157 are met, as the time for bank to bank from  $-30^\circ$  to  $30^\circ$  is  $2.9\,\mathrm{s}$ , see Fig. 8.



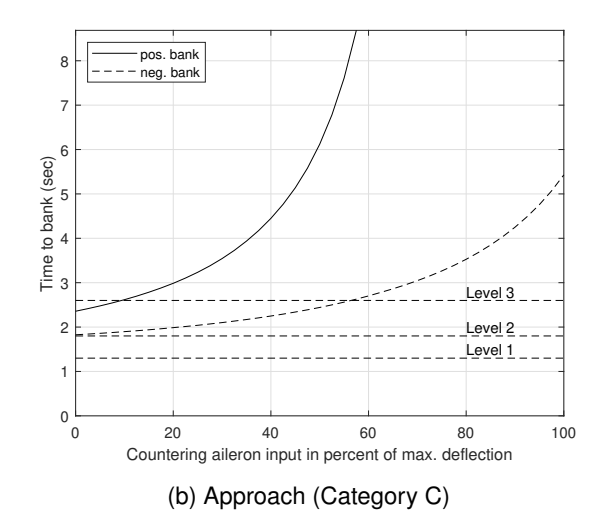


Figure 7 – Effect of countering mech. aileron deflections on time to bank, target bank angles are  $60^{\circ}$  for cruise,  $30^{\circ}$  for approach

Fig. 7 shows the effect of countering pilot aileron inputs on the time to bank. Again, these are expected to be caused unintentionally by a pilot in critical medical condition. As can be seen, the roll time quickly exceeds Level 3 qualities for the critical positive bank case. If, however, considering the certification requirements for very light aircraft, countering inputs of mechanical control surface of up to  $40\,\%$  are bearable, compare Fig. 8(a). Obviously, as all control surfaces were designed for nearly balanced control authority, the time to bank grows exponentially towards full countering deflection of pilot controls.

Table 3 – Test conditions for cruise and approach

Variable	Cruise	Approach
h in m	1000	100
$V$ in $\mathrm{km}\mathrm{h}^{-1}$	126	80
$\delta_f$ in $^\circ$	0	40
Bank angle $\phi$ in $^\circ$	60	30

The effect of FCS aileron hardover failures on the remaining pilot control authority is investigated in Fig. 8(b). Similar to the elevator, the two FCS aileron surfaces are controlled by separate actuators, wherefore the failure is expected to only affect one of the two control surfaces. The effect of a single deflected counteracting aileron on the time for bank to bank is small (see Fig. 8(b)), as the control authority remains with the pilot. Even for hardover failures, the CS-VLA requirements are met. The effect of failure can again be suppressed by a mirrored deflection of the operational FCS aileron.

#### 3.3.1 Aileron (re-)sizing

In contrast to the elevator, the distribution of aileron surface size between FCS and pilot controls is a free design variable. In the initial design, the surface area was divided equally, leading to a slightly

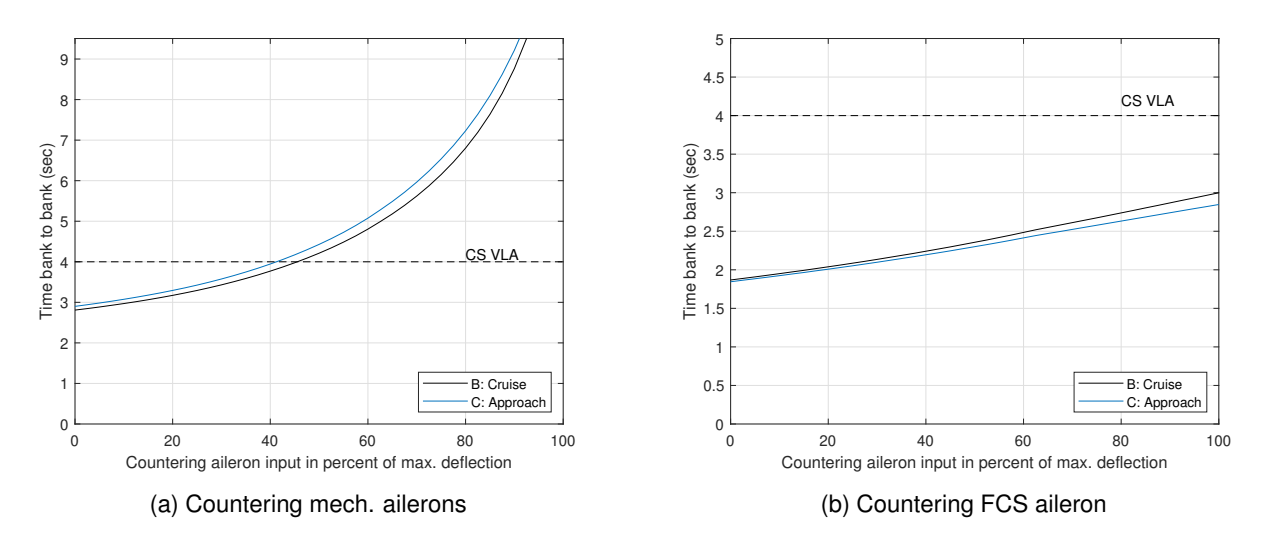


Figure 8 – Effect of countering aileron deflections on time for bank to bank (from  $-30^{\circ}$  to  $30^{\circ}$ )

superior authority of outer (pilot) controls. Still, unsatisfactory pilot handling qualities were observed in Fig. 7 for roll dynamics. As the automatic flight controls are only intended as a safety backup, they could be scaled down to their minimum size in order to foster pilot control authority in nominal flight. Figure 9 shows the effect of a varying FCS aileron size, given as ratio of total assigned aileron size. In order to fulfil CS-VLA requirements,  $20\,\%$  of the control surface area would suffice. At the same time, this allows Level 1 pilot handling qualities in cruise ( $t_{\phi}=1.27\,\mathrm{s}$ ), and Level 2 in approach conditions ( $t_{\phi}=1.8\,\mathrm{s}$ ).

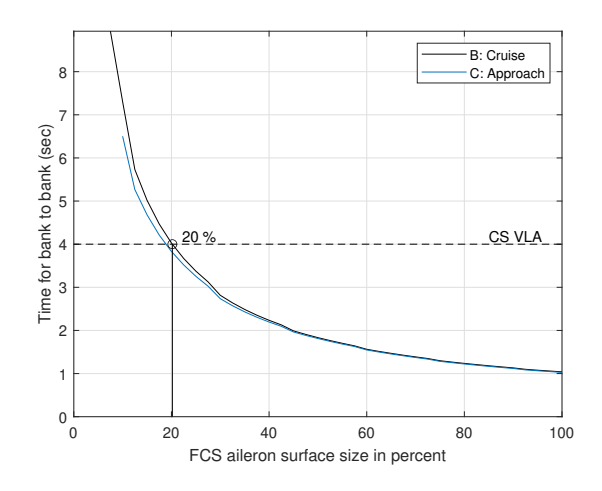


Figure 9 – Minimum FCS aileron surface size to fulfil CS-VLA 157

# 3.4 Rudder Authority Asssessment

From both handling quality and certification perspectives, cross wind takeoffs or landings and asymmetric thrust are the critical reference maneuvers for rudder authority assessment. As the latter only applies to multi-engine aircraft, we focus on steady sideslip flight. When airborne, the directional stability tends to align the aircraft with the direction of wind, resulting in zero sideslip. However, during takeoff and landing, the vehicle needs to align with the runway, wherefore a steady sideslip has to be achieved. For landings in crosswinds, the aircraft usually approaches with a sideslip of zero (crabbed approach) and needs to decrab prior to touchdown. Airbus recommends a maximum residual crab angle (angle between fuselage and runway center line) at touchdown of 5° for commercial aircraft [1].

The equation for roll and yaw moment in trimmed conditions ( $\vec{\omega}^B = \vec{0}$ ) of our aircraft model read:

$$M_{x} = \frac{\rho}{2} V^{2} \frac{b}{2} \left( c_{M_{x},\beta} \beta + c_{M_{x},\delta_{a}} \delta_{a} \eta_{\delta_{a}} + c_{M_{x},\delta_{r}} \delta_{r} \right) + Q = 0$$

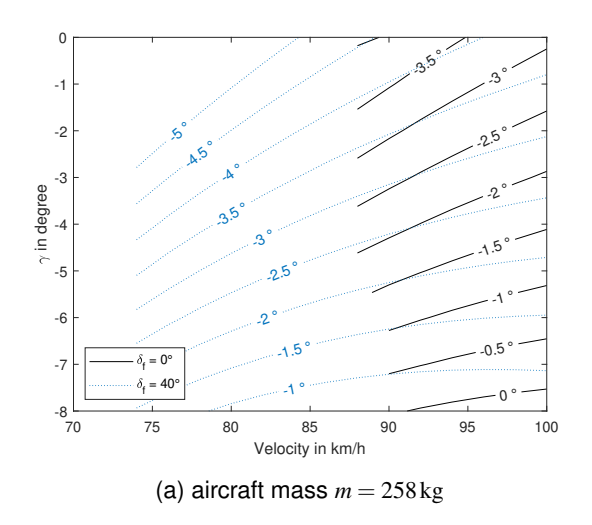
$$(12)$$

$$M_{z} = \frac{\rho}{2} V^{2} \frac{b}{2} \left( c_{M_{z},\beta} \beta + c_{M_{z},\delta_{a}} (\delta_{a} - \delta_{0})^{2} + c_{M_{z},\delta_{r}} \delta_{r} \right) = 0$$
(13)

To achieve the maximum sideslip, the rudder is fully deflected, as it is the limiting factor for the steady sideslip maneuver. The propeller torque Q is proportional to the throttle settings, which depends on the current flight state in form of, e.g., velocity V, flight path  $\gamma$ , and flap settings. With the rudder deflection  $\delta_r$  at its maximum value  $(\hat{\delta}_r)$ , and the sideslip angle to be maximized, the aileron deflection  $\delta_a$  is primarily deployed to counter the propeller torque in Eq. (12). At the same time, the yaw moment due to aileron deflection is small compared to rudder deflections. The torque balancing aileron deflection can be neglected in Eq. (13), which yields:

$$\beta_{\text{min/max}} \approx \pm \hat{\delta}_r \frac{c_{M_z, \delta_r}}{c_{M_z, \beta}}$$
(14)

According to [9], no more than 75% of roll and yaw control authority should be required to maintain a steady sideslip  $\beta$ . If only deploying the upper FCS-controlled rudder with 75% of its maximum deflection, that yields a maximum sideslip angle of  $7.7^{\circ}$  (for comparison, jointly deploying upper and lower rudder yields a max. sideslip of  $15.9^{\circ}$ ). The deviation from this value observed in trim analysis due to the neglected aileron term remains below 0.5%. The resulting aileron deflections are plotted in Fig. 10 for two different aircraft masses and varying descent angles  $\gamma$ , and show sufficient margin until saturation occurs.



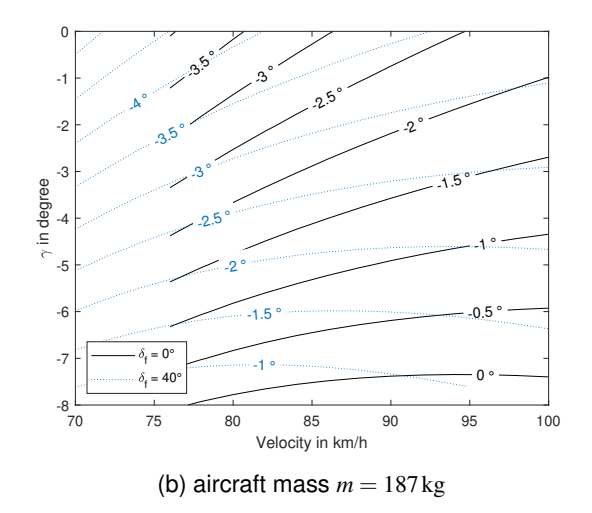


Figure 10 – Aileron deflections  $\delta_a$  for two different aircraft masses to achieve steady sideslip flight at maximum/minimum  $\beta_{\min/\max}$ 

According to CS-VLA 233, the aircraft should be capable to land in  $90^\circ$  crosswinds of 10 knots. With an approach speed of 43 knots  $(80 \, \mathrm{km} \, \mathrm{h}^{-1})$  that corresponds to a sideslip of  $\approx 13.5^\circ$ , which is close to the maxmimum sideslip for combined deflections. However, even if a maxmimum residual crab angle of  $5^\circ$  is included, the FCS rudder alone does not fullfil the crosswind landing requirement. Nevertheless, in contrast to [9], CS-VLA 233 does not prescribe to limit the surface deflections to  $75\,\%$ . Although the rudder effectiveness is decreased to  $85\,\%$  at full deflections, this still allows to fulfil the CS-VLA 233 requirement, achieving a steady sideslip of  $8.7^\circ$ . However, including the max. residual crab angle, this result only shows little margin with regard to the requirement, and consequently leaves no opportunity to vary the distribution of separated rudder surface sizes.

In case of a counteracting mechanic rudder, the boundaries of max./min. sideslip angle depend approximately linearly on the mechanic rudder deflection  $\delta_{r,l}$ . Equation (14) has to be extended by the disturbing term as follows:

$$\beta_{\text{min/max}} \approx \pm \hat{\delta}_{r,u} \frac{c_{M_z,\delta_{r,u}}}{c_{M_z,\beta}} + \delta_{r,l} \frac{c_{M_z,\delta_{r,l}}}{c_{M_z,\beta}}$$

$$\tag{15}$$

The sideslip remains trimmable until  $\delta_{r,l}\approx\pm20^\circ$ , above which flight with constant sideslip angle is unavoidable. Counteracting rudder deflections severely diminish crabbed landing capabilities in crosswinds. Alternatively, a *steady sideslip* approach, as described in [1], can be conducted. Here, a steady bank angle rotates the lift vector into the wind to align the flight path with the runway.

### 4. Discussion

The investigation of the split elevators shows that longitudinal control authority might be critically reduced. Depending on the position of the CG, elevator saturation, instead of the angle of attack, might limit the trim flight envelope. Consequently, also the pitch up maneuverability is impaired. In addition, the aircraft cannot be trimmed for a pitch angle of zero during takeoff. There are three ways to address this issue:

- 1. extend elevator deflection limits to  $\pm 30^{\circ}$ , this has already shown to be effective in the analysis
- 2. increase the control surface chord, so far the surface chord was 20% of wing chord
- 3. use the FCS surfaces to augment pilot commands (i.e. copy the deflection of mechanical control surfaces), especially during the critical takeoff maneuver

It was shown that untreated failures of an FCS elevator drastically reduce the flight envelope, especially affecting the low speed region. This can be easily compensated by the remaining operational FCS elevator surface, however, at the expense of pilot augmentation capability in case of hardover failures. In contrast, erroneous pilot elevator inputs quickly degrade the longitudinal control power. The balance of control authority was, however, the initial design principle. The FCS is intended as a backup system to avoid early deployment of the rescue parachute. Nevertheless, this option remains in case of unresolvable failure conditions.

In contrast to the elevator, both aileron systems show sufficient control authority to fulfil certification requirements. Still, the mechanical controls alone provide unfavorable pilot handling quality levels, which might decrease the willingness to fly such an aircraft. In addition to pilot control augmentation (again FCS surfaces would imitate pilot controls), a resizing of the FCS aileron surface could address this issue. Sizing the aileron exactly at the boundary of certification requirements significantly improves pilot control authority. However, this comes at the expense of failure robustness. For the current equally distributed surface sizes, failure on the FCS side are uncritical, even if untreated, whereas erroneous pilot inputs can be handled until  $40\,\%$  of maximum deflection. Above that, the aircraft is no longer controllable and the rescue parachute has to be deployed.

Landing in strong crosswinds shows to be challenging but possible with split rudder surfaces. For the crosswinds mentioned in certification requirements, a residual crab angle (within reasonable limits) at touchdown has to be accepted. Again, pilot augmentation would improve handling qualities. For counteracting surface deflections in failure cases, control authority quickly decreases and the decrab maneuver cannot be performed any longer. As an alternative to the deployment of the rescue parachute, a steady sideslip approach as described in [1] could be conducted.

#### 5. Conclusion

This paper introduced a mixed flight control layout, where control surfaces are separated to share control authority between pilot and an automated flight control system. The latter is intended primarily as a safety backup in case of (medical) emergencies. The investigation of the flight and handling qualities for the single systems shows that, depending on the position of the CG, especially the longitudinal control power might become critical. In contrast, the lateral motion (especially roll dynamics) meets certification requirements, but results in unsatisfying pilot handling qualities. These issues can be addressed with flight control augmentation. In a rudimentary approach, the FCS surfaces copies the deflections of pilot-controlled mechanic surfaces, which leads to the same flight characteristics as the aircraft with standard control surface configuration. Above that, advanced safety functions, like stall prevention, could be developed and introduced in the future. The basic result of the investigation of the mixed flight control layout is that, despite the decreased performance, the FCS control authority suffices to control and safely land the aircraft in case of emergencies.

#### 6. Contact Author Email Address

marc.may@dlr.de daniel.milz@dlr.de

# 7. Acknowledgments

The funding of the *MOREALIS* project within the LUFO VI-1 framework (FKZ: 20Q1935E) by the German Federal Ministry for Economic Affairs and Climate Action (BMWK), is gratefully acknowledged.

Supported by:



on the basis of a decision by the German Bundestag

# 8. Copyright Statement

The authors confirm that they, and/or their company or organization, hold copyright on all of the original material included in this paper. The authors also confirm that they have obtained permission, from the copyright holder of any third party material included in this paper, to publish it as part of their paper. The authors confirm that they give permission, or have obtained permission from the copyright holder of this paper, for the publication and distribution of this paper as part of the ICAS proceedings or as individual off-prints from the proceedings.

# **Appendix**

#### 8.1 Aerodynamic Coefficient model

The non-dimensional rotational rates in Table 2 are defined as:

$$\begin{bmatrix} p^* \\ q^* \\ r^* \end{bmatrix} = \frac{1}{V} \begin{bmatrix} p\frac{b}{2} \\ q\overline{c} \\ r\frac{b}{2} \end{bmatrix}$$
 (16)

, using aircraft spanwidth b and mean aerodynamic chord  $\overline{c}$ . If required for a better fit, the aerodynamic state is adapted, i.e. to include non-linearities. The adaption of the respective states is presented in the following:

Starting with the drag state, a deviation of the angle of attack  $\alpha$  or sideslip  $\beta$  from zero configuration should always increase the drag. In addition, according to Glauert's linear profile theory [13], the drag due to flap deflection can be modelled as:

$$\Delta c_{D\delta i} = k_d c_{L\alpha} \alpha_\delta \delta_i \sin \delta_i = c_{D\delta} \cdot \delta_i \sin \delta_i \tag{17}$$

The drag state is changed accordingly

Table 4 – Adaptation of aerodynamic state for  $\vec{x}_A$  for drag computation

ID	Variable		
3	$(\alpha - \alpha_0)^2$		
4	$oldsymbol{eta}^2$		
8 - 19	$\delta_i \sin \delta_i$		

Due to the dihedral of the main wing, an asymmetric deflection of ailerons or flaps will result in a side force which is proportional to the change in lift. As described below for the lift coefficient, the increase in lift due to surface deflection is a function of flap efficiency  $\eta_{\delta}$ , which is decreasing with higher deflections.

Table 5 – Adaptation of aerodynamic state for  $\vec{x}_A$  for side force computation

ID	Variable	
8 – 13	$\eta_{\delta_i} \cdot \delta_i$	

The contribution of all horizontal control surfaces to the lifting force is corrected with the surface efficiency.

Table 6 – Adaptation of aerodynamic state for  $\vec{x}_A$  for lift computation

ID	Variable	
8 – 17	$\eta_{\delta_i} \cdot \delta_i$	

If deflected asymmetrically, the same applies for the rolling moment, wherefore the aerodynamic state for the roll moment is the same as the one for lift in Table 6.

The change in downwash due to flap deflection causes a quadratic response of the pitching moment. In addition, the deflection of the rudder changes the induced drag at the vertical tailplane, which is likewise a quadratic function.

Table 7 – Adaptation of aerodynamic state for  $\vec{x}_A$  for pitching moment computation

ID	Variable
10, 13, 18, 19	$\delta_i^2$

In a similar way, a control surface deflection at the main wing (aileron or flap) increases the lift, and therefore also causes in increase in induced drag. If deflected asymmetrically, the difference in induced drag creates a yawing moment with a quadratic response to the deflection. However, the aifoil is cambered, and therefore the induced drag increases from the zero lift deflection  $\delta_0$ . The same applies to the elevator, but the horizontal tailplane deploys an uncambered NACA0009.

Table 8 – Adaptation of aerodynamic state for  $\vec{x}_A$  for yawing moment computation

ID	Variable
8 - 13	$(\delta_i - \delta_0)^2$
14 - 17	$(\delta_i)^2$

The total coefficient for aerodynamic forces or moments are found by element-wise multiplication of the aerodynamic state with a coefficient vector. In addition, the lift coefficient is corrected with a stall correction in the form

$$c_{L,\text{eff}} = c_L \cdot f_{\text{stall}} \tag{18}$$

$$f_{\text{stall}} = \frac{c_{L, \text{profile}}(\alpha)}{c_{L\alpha}\alpha}$$
 (19)

where  $c_{L,\text{profile}}$  is the lift coefficient of the main airfoil, GA(W)2. Furthermore, the resulting lift coefficient is used to compute the induced drag which is then added to the drag obtained by the coefficient vector  $\vec{c}_d$ .

$$c_D = \vec{c}_D^T \cdot \vec{x}_{A,D} + \frac{c_{L,\text{eff}}^2}{\pi \Lambda} \tag{20}$$

with aspect ratio  $\Lambda = b^2/S$  and the adapted aerodynamic state for drag computation  $\vec{x}_{A,D}$ . The following geometry data is used for the aerodynamic model:

Table 9 – Aircraft model data

Parameter	
b	6.4 m
$\overline{c}$	0.9719 m
S	$6.12\mathrm{m}^2$
	$\overline{c}$

The aerodynamic reference point is located at

$$\vec{r}_{AC} = \begin{bmatrix} 1.5896 & 0 & 0.8488 \end{bmatrix}^T$$
 (21)

relative to the reference point (defined to be located in the x-z-plane, horizontally at propeller tip and vertically at height of the ground). This coincides with the center of gravity at maximum take-off loading. Depending on the setup, the horizontal position can vary from  $1.561\,\mathrm{m}$  to  $1.665\,\mathrm{m}$ , while the mass varies between  $m = 203\,\mathrm{kg}$  and  $m = 258\,\mathrm{kg}$ .

### 8.2 Coefficient Model Comparison

Fig. 11 shows the comparison of the derived coefficient model and the strip theory model.

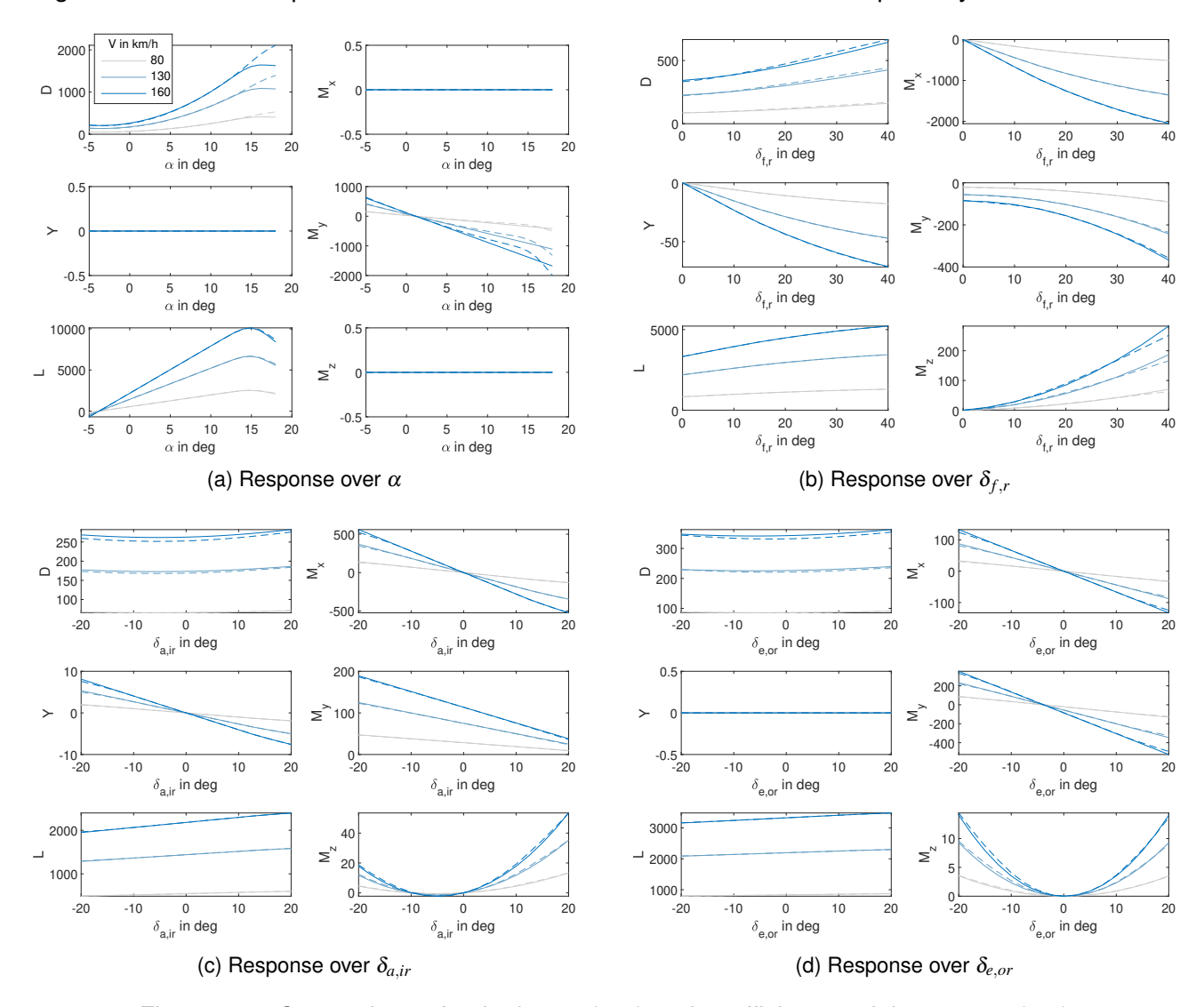


Figure 11 – Comparison of strip theory (- - -) and coefficient model response (---)

#### References

- [1] Airbus. Crosswind landings flight operations briefing notes. Technical report, Airbus, 2008.
- [2] W. R. Bolton and D. J. Collins. General aviation application of separate surface stability augmentation. *Journal of Aircraft*, 12(10):826–829, October 1975. ISSN 1533-3868. doi: 10.2514/3.59877.
- [3] Bernd Chudoba and Michael Cook. Identification of design-constraining flight conditions for conceptual sizing of aircraft control effectors. In AIAA Atmospheric Flight Mechanics Conference and Exhibit. American Institute of Aeronautics and Astronautics, June 2003. doi: 10.2514/6. 2003-5386.
- [4] George Cooper and Robert Harper. The use of pilot ratings in evaluation of aircraft handling qualities. *NASA Ames Technical Report*, 05 1969.
- [5] EASA. Easy access rules for normal, utility, aerobatic and commuter category aeroplanes (cs-23), 2018.
- [6] FAA. Far part 23 and part 25. Washington, D.C.
- [7] M. G. Goman, A. V. Khramtsovsky, and E. N. Kolesnikov. Evaluation of aircraft performance and maneuverability by computation of attainable equilibrium sets. *Journal of Guidance, Control,* and Dynamics, 31(2):329–339, March 2008. ISSN 1533-3884. doi: 10.2514/1.29336.
- [8] Philippe Goupil. Airbus state of the art and practices on fdi and ftc in flight control system. *Control Engineering Practice*, 19(6):524–539, June 2011. ISSN 0967-0661. doi: 10.1016/j. conengprac.2010.12.009.
- [9] J. Kay, W.H. Mason, W. Durham, and F. Lutze. Control authority assessment in aircraft conceptual design. In *AIAA Aircraft Design*, *Systems*, and *Operations Meeting*, 1993.
- [10] Deutsche Luftverkehrs-Zulassungs-Ordnung (LuftVZO). § 1 Zulassungspflicht und Umfang der Zulassung. https://www.gesetze-im-internet.de/luftvzo/\_\_1.html.
- [11] MIL-F-8785C. Flying qualities of piloted airplanes, 1980.
- [12] MIL-STD-1797. Flying qualities of piloted vehicles, 1997.
- [13] Erik D. Olson. Semi-Empirical Prediction of Aircraft Low-Speed Aerodynamic Characteristics. In *53rd AIAA Aerospace Sciences Meeting*, 2015. doi: 10.2514/6.2015-1679.
- [14] Brian Pagán, Alex de Voogt, and Robert Doorn. Ultralight aviation accident factors and latent failures: A 66-case study. *Aviation, space, and environmental medicine*, 77:950–2, 09 2006.
- [15] J. Roskam and S. Henry. An approach to the synthesis of separate surface automatic flight control systems. In *Guidance and Control Conference*. American Institute of Aeronautics and Astronautics, August 1973. doi: 10.2514/6.1973-834.
- [16] Jan Roskam and Samuel Henry. Synthesis of a separate surface wing leveler. *Journal of Aircraft*, 11(11):657–658, November 1974. ISSN 1533-3868. doi: 10.2514/3.60400.
- [17] Mohammad Sadraey and Richard Colgren. A systems engineering approach to the design of control surfaces for uavs. In 45th AIAA Aerospace Sciences Meeting and Exhibit. American Institute of Aeronautics and Astronautics, January 2007. doi: 10.2514/6.2007-660.
- [18] Michael J. See and David Levy. The state of the art of general aviation autopilots. Technical report, NASA, 1980.

### MOREALIS – enhanced safety for micro-aircraft operations

- [19] Christian Weiser and Daniel Ossmann. Fault-tolerant control for a high altitude long endurance aircraft. *IFAC-PapersOnLine*, 55(6):724–729, 2022. ISSN 2405-8963. doi: 10.1016/j.ifacol. 2022.07.213.
- [20] Peter Zaal, Daan Pool, Alexander in 't Veld, Ferdinand Postema, Max Mulder, Marinus van Paassen, and Jan Mulder. Design and certification of a fly-by-wire system with minimal impact on the original flight controls. In *AIAA Guidance, Navigation, and Control Conference*. American Institute of Aeronautics and Astronautics, June 2009. doi: 10.2514/6.2009-5985.